Ultrasonics 50 (2010) 798–802

Contents lists available at ScienceDirect

Ultrasonics

journal homepage: www.elsevier.com/locate/ultras

Visualization and minimization of disruptive bubble behavior in ultrasonic field

Wonjung Kim [a], Keunhwan Park [a], Jongkeun Oh [b], Jaehyuck Choi [b], Ho-Young Kim [a,*]

[a] School of Mechanical and Aerospace Engineering, Seoul National University, Seoul 151-744, Republic of Korea
[b] Semiconductor Business, Samsung Electronics, Yongin, Gyeonggi 449-711, Republic of Korea

ARTICLE INFO

Article history:
Received 2 October 2009
Received in revised form 25 March 2010
Accepted 7 April 2010
Available online 18 April 2010

Keywords:
Ultrasonic cleaning
Bubble oscillation
Acoustic pressure
Adhesion force

ABSTRACT

Although ultrasonic technology has been successfully adopted for semiconductor cleaning, a recent trend of extreme miniaturization of patterns calls for a novel process that can remove contaminant particles without damaging nanoscale patterns. Unstable bubble oscillations have been hypothesized to cause such surface damages, and here we show direct visualization results that a high acoustic pressure induces bubble instability leading to pattern damages. As a remedy for the conventional ultrasonic cleaning scheme, we introduce a novel cleaning system using dual transducers, in which one transducer generates bubbles with a high acoustic pressure in an acoustically isolated sub-chamber and the other drives the oscillation of bubbles around the cleaning area at a low acoustic pressure. The system is shown to achieve a high cleaning efficiency for submicron-sized particles while significantly suppressing the disruptive bubble instability thereby reducing the detachment of firmly attached nanoparticles. Comparison of the adhesion force of the firmly attached nanoparticles and the yield strength of nanopatterns allows us to anticipate that this scheme is capable of reducing damages of nanopatterns on semiconductor wafers and photomasks.

© 2010 Elsevier B.V. All rights reserved.

1. Introduction

In semiconductor manufacturing, contaminants from various sources, such as photoresists, solvents, and containers can deposit on wafers and photomasks, which eventually lead to yield loss unless removed [1]. Megasonic cleaning using acoustic waves of the frequency on the order of 1 MHz has been widely employed for over decades to remove the micron- or submicron-sized contaminant particles [2]. However, as the feature size shrinks down to less than 100 nm, the mechanical strength of the structures gets sometimes too low to endure the removal force of the conventional megasonic cleaning processes, resulting in damages as shown in Fig. 1. Therefore, preventing damages of extremely thin patterns while almost completely removing contaminant particles is one of the most challenging tasks in the semiconductor cleaning processes.

Recently, the mechanism of cleaning by megasonic waves was elucidated by directly visualizing the particle removal process [3]. It was shown that particles are detached from a solid surface due to oscillating cavitation bubbles. The bubble oscillation generates a local pressure gradient, which attracts particles toward the bubble interface. The magnitude of the local pressure gradient increases with the bubble oscillation amplitude, which in turn increases with the acoustic pressure input. Combined with the fact that the number of bubbles rises with the acoustic pressure, the cleaning efficiency can be enhanced by increasing the acoustic amplitude. On the other hand, no visualization results have been reported to date showing how patterns are damaged in megasonic cleaning processes. However, in the absence of ultrasonic effects, cavitation bubbles were experimentally observed to collapse near a solid generating a fast liquid jet toward the wall [4,5]. Under the effects of ultrasound, although not observed experimentally so far, the unstable bubble oscillation that causes liquid jets to penetrate microbubbles was predicted by numerical computations [6,7]. Also, such instability was computed to be promoted by the increase of the acoustic pressure, P_a [7]. Based on the experimental observations of crater shapes on substrates [8–10], the bubble instability is considered to cause damages in cleaning. Still, there have been no direct visualization experiments to confirm these postulates.

The foregoing results, although hypothetical, suggest that a high acoustic pressure does not only enhance cleaning but also promotes pattern damages at the same time. Thus the conventional cleaning systems employing only a single transducer suffers from a dilemma: although P_a should be reduced to prevent unstable bubble oscillation [12], the lowered P_a deteriorates the cleaning efficiency. As a first step to solve this problem, in this work we start with verifying experimentally that unstable bubble oscillations are indeed caused by a high acoustic pressure amplitude using a high-speed imaging technique. Then we propose a novel cleaning

* Corresponding author. Address: Rm 302-423, Seoul National University, Gwanak, Seoul 151-744, Republic of Korea. Tel.: +82 2 880 9286; fax: +82 2 880 9287.
E-mail address: hyk@snu.ac.kr (H.-Y. Kim).

0041-624X/$ - see front matter © 2010 Elsevier B.V. All rights reserved.
doi:10.1016/j.ultras.2010.04.002

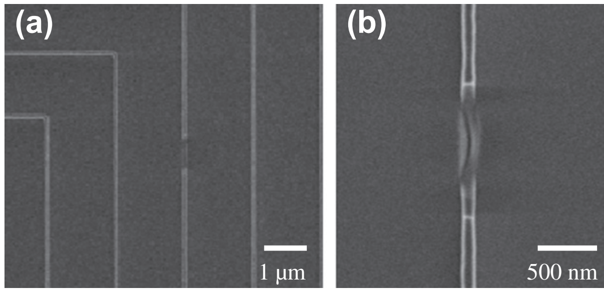

Fig. 1. Scanning electron microscopy (SEM) images of damaged photomask patterns (Cr on quartz) with 120 nm in width.

system that is deprived of violently oscillating bubbles while still maintaining a high particle removal efficiency (PRE), and experimentally show its effectiveness.

Besides those industrial processes, such biotechnologies as diagnostic ultrasound imaging and drug delivery utilize (encapsulated) microbubbles subjected to ultrasonic irradiation [9]. Thus it is possible that unstable oscillations of these bubbles near surfaces lead to damages of tissues or cells, which are harmful in most cases. On the other hand, disruption of cell membranes due to an ultrasonic bubble can be used for introducing drugs to the interior of cells. Hence, understanding and controlling the disruptive potential of ultrasonic bubbles are of crucial importance in biologically relevant fields as well.

2. Visualization of disruptive bubble oscillations

We first verified the postulate that a high P_a leads to unstable bubble oscillation and jet formation, which was not experimentally visualized to date. We used an apparatus as shown in Fig. 2a. The setup consists of a quartz bath, on one of whose sides a piezoelectric transducer is attached, an upright microscope (Olympus BX-51M) with a water immersion objective lens (Olympus LUMPLFL 40XW), and a high-speed camera (Photron APX-RS). In the experiments, piezoelectric transducers with two different resonance frequencies (f_r), 170 kHz and 950 kHz, were employed. A vertical wall was situated below the objective lens to observe the interaction of a bubble with the solid. Acoustic pressure amplitude was measured by a needle hydrophone (Precision Acoustics HPM1/1).

The images of oscillating bubbles on the vertical wall are shown in Fig. 2b–d, where a transducer with f_r = 170 kHz was used. A bubble exhibits stable oscillations for a low P_a of 68 kPa as in Fig. 2b. As P_a increases to 114 kPa, the oscillation gets unstable causing a liquid jet to penetrate the bubble interface as in Fig. 2c. As we further increase P_a to 132 kPa, Fig. 2d, the oscillation becomes so vigorous that multiple dents are formed at the gas–liquid interface with the axial symmetry broken. The second frame in Fig. 2d shows a water layer (or column) squeezed between daughter bubbles that result from splitting of an original bubble of the first frame. Such a water column was observed for a microbubble driven in the ultrasonic field at the frequency of 1 MHz. [11] On the other hand, the water jet penetrating the toroidal bubble in the second frame of Fig. 2c is almost undistinguishable from a jet produced by a collapse of a millimeter-sized bubble nucleated by laser irradiation [5]. Such a jet generated in the ultrasonic field is reported here for the first time to the authors' knowledge. Our experimental results indeed show that bubble oscillations get unstable as P_a increases, which exerts a large stress on a solid surface [5] raising the possibility of damaging nanostructures.

To check whether a violently oscillating bubble indeed damages a pattern on a wafer surface, we fabricated linear arrays of silicon walls with 3 μm and 0.7 μm in height and width, respectively, by deep reactive ion etching as shown in Fig. 3. In this experiment, we used a transducer with f_r = 950 kHz and the acoustic pressure amplitude was as high as P_a = 250 kPa. Although it is impossible to predict when and where a bubble will emerge and which pattern it will break, we succeeded in capturing the moment of a bubble breaking a pattern by continually observing a selected area (30 μm × 30 μm) with a high-speed camera (running at 10,000

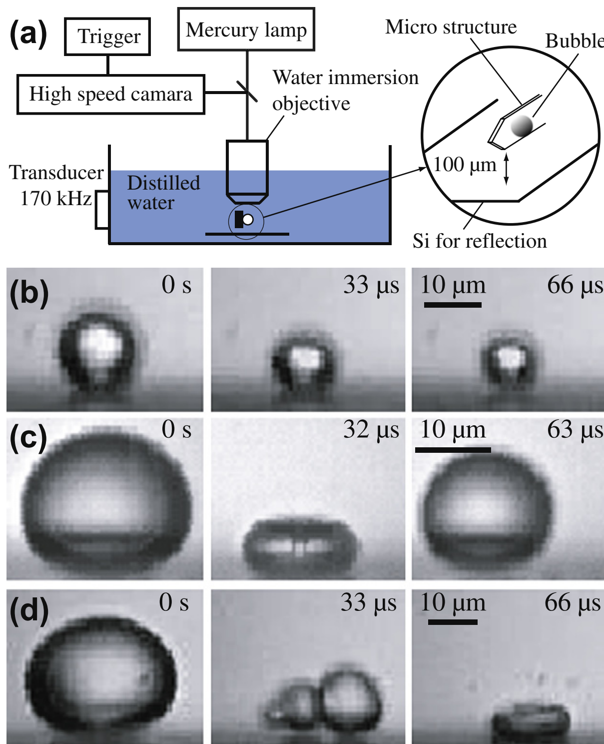

Fig. 2. (a) Schematic of the bubble visualization apparatus. (b) Stable bubble oscillation at P_a = 68 kPa. (c) Unstable bubble oscillation at P_a = 114 kPa. (d) Vigorous and unstable bubble oscillation at P_a = 132 kPa.

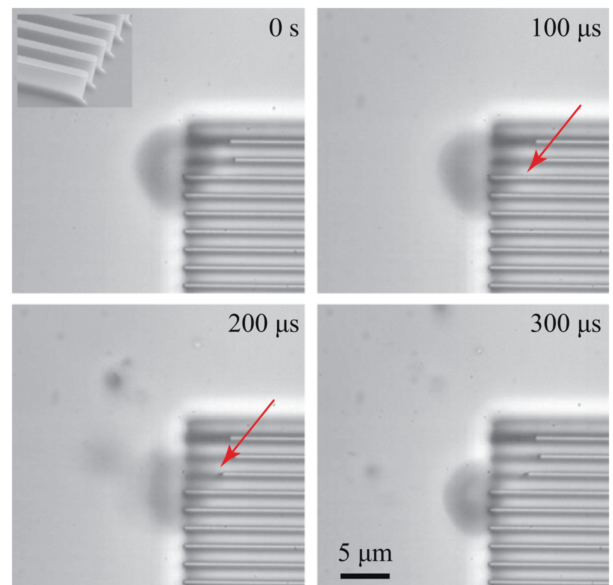

Fig. 3. High-speed images of an ultrasonic bubble breaking a Si line pattern. The edge of a pattern designated by an arrow is fractured by the bubble within a time much shorter than 100 μs. Inset: SEM image of the line patterns.

frames per second) until a desired event occurs. As shown in Fig. 3, a bubble that oscillates around the edge of the third row of the linear patterns breaks a part of the pattern leaving a damage. Although the breaking process takes place so fast that the currently adopted high-speed camera is unable to resolve intermediate steps, this is the first reported direct visual evidence that a bubble causes a pattern damage.

So far, we have shown that a violent bubble oscillation is caused by a high acoustic pressure amplitude and that it exerts disruptive impact on substrates. This then leads us to conclude that reducing P_a in the cleaning process is essential to suppress the bubble violence and consequently to minimize pattern damages. In the next section, we propose a novel means to decrease P_a while preserving a high removal efficiency of submicron-sized particles.

3. Dual-ultrasonic scheme

At first glance, the simplest approach to avoid the pattern damage while achieving a high PRE would be to adjust P_a such that the force of bubbles acting on a solid lies between the mechanical stiffness of patterns and the minimum particle removal force. However, it has the following problems. As the pressure distribution in a megasonic cleaner is very complicated due to near-field effects [13] and waves scattering on bubbles and bath walls, the bubble forces have wide ranges even at a fixed acoustic pressure input. Thus it is virtually impossible to delicately tune the bubble forces within a narrow range. In addition, excessively reducing acoustic pressure level to avoid the damage of ever-shrinking patterns may eventually fail to even induce cavitation.

Therefore, we propose a novel scheme which keeps the high number density of bubbles with one transducer (which typically involves many unstably oscillating bubbles due to increased P_a when a single transducer is used) while reducing the acoustic pressure that drives the bubble oscillation with another transducer. That is, the generation of bubbles and the excitation of bubble oscillation are decoupled by using dual transducers, as shown in Fig. 4. In the system, acoustic fields around the two transducers (both having the resonance frequency of 0.95 MHz) are isolated by an air layer because acoustic waves are reflected on the interface having density difference [14]. The transducer I, responsible for bubble generation, generates a high P_a within a sub-chamber and a resulting bubbly fluid is pumped at a rate of 37 cm^3/s through a nozzle with 5 mm in diameter, to the main chamber. The transducer II is driven at an amplitude low enough to prevent unstable bubble oscillations but high enough to keep stable oscillations. In this manner, we can accommodate a high number density of bubbles that oscillate stably in the main cleaning chamber.

We tested whether the dual transducer system could achieve a high PRE at a significantly lower P_a than a single transducer system. Contaminant particles, fluorescent spherical polystyrene latex (PSL) particles with 520 nm in diameter, were attached by an atomizer as mixed with isopropyl alcohol to a quartz photomask coated with Cr. Then we waited 5 h to regulate the adhesion force before immersing the photomask in de-ionized (DI) water. To find the dependence of the PRE of a single transducer system on P_a, we varied the input voltage to the transducer II with the transducer I off. The PRE, defined as the ratio of the number of removed particles to that of originally deposited particles, was obtained through image analysis for each P_a. Fig. 5a shows that the PRE increases with P_a, starting from 22% at P_a = 68 kPa and reaching 97% at P_a = 114 kPa. Then the PRE is saturated despite the increase of P_a. In all the cases, the cleaning was performed for 3 min. The dramatic increase of the PRE in the range P_a = 80 − 100 kPa coincides with the sudden burst of cavitation in the same range of P_a. On the other hand, when the transducer I is turned on to generate bubbles at the acoustic pressure of 197 kPa within the sub-chamber, a PRE of 97% was achieved with the transducer II operating at P_a = 68 kPa only. It is again noted that since the acoustic field due to the transducer I is isolated by an air layer, the cleaning area is affected only by the field induced by the transducer II. We show in Fig. 5b that omitting any one component in the dual-transducer system results in a PRE much lower than 97%. The images of the fluorescent particles on the photomask, Fig. 6, clearly show that a low P_a from the transducer II can remove 520-nm diameter particles effectively when the transducer I is used together.

Upon verifying that a high PRE of 520 nm-diameter particles can be achieved at a low P_a with a dual transducer system, we tested the capability of the system in reducing disruptive effects of bubbles on surfaces compared to a single transducer system. It should be noted here that damages of real nanopatterns are extremely difficult to quantify due to the technical problem of finding and counting damaged patterns with about 100 nm in width over a wide photomask or wafer area through SEM. In the actual photo-

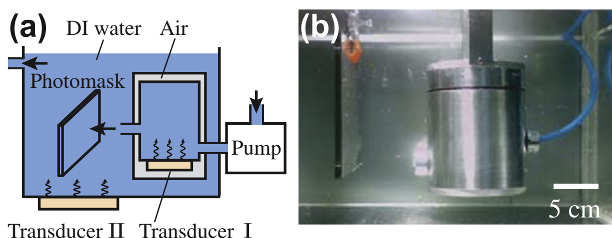

Fig. 4. (a) A schematic and (b) a photograph of a dual-transducer cleaning system.

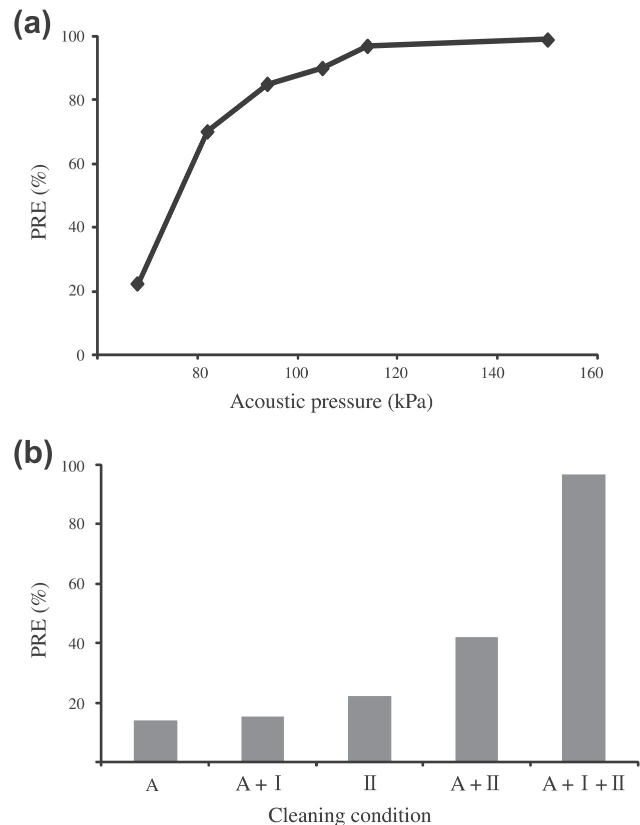

Fig. 5. (a) Effects of the acoustic pressure on the PRE of 520-nm diameter particles when a single transducer II is used. (b) PRE's obtained by various operation conditions. The letter A denotes the liquid stream due to a pump toward the photomask and I and II denote the transducer that is turned on.

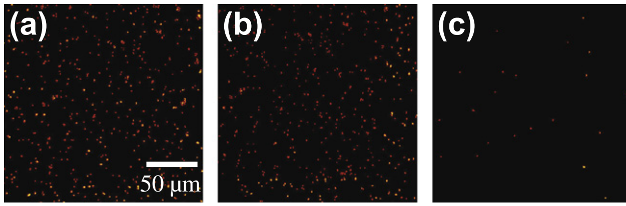

Fig. 6. Fluorescent images of 520 nm-diameter PSL particles on photomask. (a) Before cleaning. (b) The surface cleaned with the transducer II (68 kPa) only. (c) The surface cleaned with the dual system.

mask manufacturing processes, only dozens of one million lines are damaged through megasonic cleaning, and reducing the number to less than about 30 out of a million is currently pursued. Thus we instead investigated the detachment probability of PSL particles with the diameter of 48 nm that were firmly attached to the substrate to have the comparable adhesion strength to that of nanopatterns. We let the particles in contact with the photomask for 48 h before cleaning to induce large deformation that enhances the adhesion strength. The adhesion force of the particle due to van der Waals interaction [3] is given by $F_a = \frac{1}{6}AR/Z_0^2(1 + a^2/RZ_0)$, where A is the Hamaker constant, R the particle radius, Z_0 the distance between the particle and the flat surface, normally taken to be approximately 0.4 nm [15], and a the particle-substrate contact radius [16]. For PSL particles on Cr surface immersed in water, A is calculated to be 1.6×10^{-20} J [17–20]. The degree of particle deformation determining a depends on the particle rigidity and the duration of contact. Using an atomic force microscope (AFM, Park Systems XE-70), a was measured to be approximately 0.6R after 48 h of attachment. Then the adhesion torque of the 48 nm-diameter particles is $\tau_{a,1} \sim aF_a \sim 1.2 \times 10^{-16}$ N m. Comparing the adhesion torque $\tau_{a,1}$ with the removal torque exerted by a stably oscillating bubble [3], $\tau_{r,1} \sim (8\pi/3)\rho\omega^2R^4R_b \sim 3 \times 10^{-19}$ N m, where ω being the angular frequency of ultrasound and R_b the resonant bubble radius (3 μm according to Minnaert's formula [14]), we find that $\tau_{r,1}$ is orders of magnitude smaller than $\tau_{a,1}$. Thus stably oscillating bubbles can hardly detach the nanoparticles.

We compare this adhesion strength with the mechanical strength of a nanopattern under a load as shown in Fig. 7. When the force F is exerted on the structure, the maximum stress occurring at the clamped bottom becomes $\sigma_m = 6hF/bw^2$ where w is the width, b the length, and h the height [21]. For the rectangular structure whose frontal area (bh) is the same as the cross-sectional area of the particle ($\sim\pi R^2$), $b \sim \pi R^2/h$, so that $\sigma_m \sim 6h^2F/\pi R^2w^2$. In order for the structure to resist F, σ_m should not exceed σ_Y, the yield strength, the aspect ratio of the structure is bounded as $h/w \leqslant (\pi R^2\sigma_Y/6F)^{1/2}$. Assuming that the rectangular Cr pattern (having $\sigma_Y = 260$ MPa [22]) is subjected to the force comparable to the adhesion force of the 48 nm-diameter particle, $F = 8.3 \times 10^{-9}$ N, we get $h/w \leqslant 3$. This allows us to regard that the firmly attached 48 nm-diameter particles simulate a pattern of $w = 20$ nm, $h = 60$ nm and $b = 30$ nm, for example, with the similar mechanical strength.

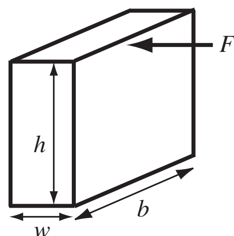

Fig. 7. A rectangular nanopattern whose shaded frontal area is the same as the cross-sectional area of the particle.

Before proceeding to the experiments using 48 nm-diameter particles, we check whether the theoretically calculated bubble force was sufficiently strong to remove previously used large particles with 520 nm in diameter. The adhesion torque is scaled as $\tau_{a,2} \sim 7 \times 10^{-16}$ N m, in which we used $a = 0.1R$ based on the AFM measurements. The removal torque for these particles is given by $\tau_{r,2} \sim 4 \times 10^{-15}$ N m, an order of magnitude higher than the adhesion torque, $\tau_{a,2}$, consistent with the fact that the 520 nm-diameter particles were almost completely removed by cavitation bubbles.

Now we describe the experimental results with firmly attached 48 nm-diameter particles. After 3 min of cleaning, the single transducer system, using the transducer II only, operated at $P_a = 114$ kPa (that achieved the PRE of 97% for 520 nm-diameter particles) resulted in the PRE of 13% for 48 nm-diameter particles, implying frequent unstable bubble oscillations that led to the detachment of the firmly attached nanoparticles. On the other hand, when the dual transducer system was used with the transducer II operated at $P_a = 68$ kPa (that achieved the PRE of 97% for 520 nm-diameter particles as well), the PRE for 48 nm-diameter particles was successfully reduced to 1%. These results support our hypothesis that the dual transducer system maintains stable bubble oscillation with the transducer II (that drives a low acoustic pressure to reduce the disruptive cleaning effect) while providing sufficiently many bubbles to the cleaning area generated by the transducer I.

4. Conclusions

In the first part of this work, we showed that bubble oscillations are destabilized when a ultrasonic field with a high acoustic pressure amplitude is applied. Also a bubble oscillating under ultrasonic field of a high acoustic pressure amplitude was shown to be capable of breaking a wafer pattern. The high-speed imaging results of microbubbles provide the first experimental evidence that their oscillation behavior can be controlled with the magnitude of acoustic pressure. This finding can be potentially applied in the biotechnology fields such as diagnostic ultrasound imaging and drug delivery as mentioned earlier.

In the semiconductor cleaning processes, lowering the acoustic pressure to suppress the disruptive bubble behavior reduces the number of cavitation bubbles that play critical roles in removing the contaminant particles. Therefore, in the second part of this work we developed a dual-transducer ultrasonic cleaning system that decouples the generation of bubbles and the excitation of bubble oscillations. By reducing the acoustic pressure amplitude while maintaining a high number density of bubbles around the cleaning area, the detachment of firmly attached nanoparticles was shown to be significantly suppressed with the high cleaning efficiency of submicron-sized particles preserved. By comparing the adhesion force of the nanoparticles and yield strength of rectangular nanopatterns, we showed that this dual-transducer scheme may provide a viable solution to reduce pattern damages. Despite the proved effectiveness of the proposed dual-ultrasonic scheme based on the experiments using submicron-sized and nano-sized particles, comparison of nanopattern damage probabilities of a conventional single-transducer scheme and of the currently proposed dual-transducer scheme is in order in the actual semiconductor manufacturing facilities.

The principle of the current megasonic cleaning scheme in selectively removing submicron-sized particles while preserving firmly attached nanoparticles on a surface is based on the difference of detachment torque exerted by bubbles which is the function of the particle size. When the detachment torque of ever-

shrinking patterns and that of nanoparticles to be removed become no longer separable in the future, a megasonic cleaning scheme alone would not be capable of selectively removing contaminant particles without damaging patterns. In this case, a chemical approach in addition to the current physical mechanism needs to be appended to selectively remove contaminant particles from nanopatterned surfaces.

Acknowledgments

This work was supported by Samsung Electronics and KRF (Grant No. KRF-J03001) and administered via SNU Engineering Research Institute.

References

[1] W. Kern, Handbook of Semiconductor Wafer Cleaning Technology, Noyes Pubications, Park Ridge, NJ, 1993.
[2] K. Bakhtari, R.O. Guldiken, A.A. Busnaina, J. Park, Experimental and analytical study of submicrometer particle removal from deep trenches, J. Electrochem. Soc. 153 (2006) C603–C607.
[3] W. Kim, T.-H. Kim, J. Choi, H.-Y. Kim, Mechanism of particle removal by megasonic waves, Appl. Phys. Lett. 94 (2009) 081908.
[4] J.P. Dear, J.E. Field, A.J. Walton, Gas compression and jet formation in cavities collapsed by a shock wave, Nature 332 (1988) 505–508.
[5] C.D. Ohl, M. Arora, R. Dijkink, V. Janve, D. Lohse, Surface cleaning from laser-induced cavitation bubbles, Appl. Phys. Lett. 89 (2006) 074102.
[6] J.R. Blake, G.S. Keen, R.P. Tong, M. Wilson, Acoustic cavitation: the fluid dynamics of non-spherical bubbles, Philos. Trans. Roy. Soc. Lond. A 357 (1999) 251–267.
[7] M.L. Calvish, O. Lindau, J.R. Blake, A.J. Szeri, Shape stability and violent collapse of microbubbles in acoustic traveling waves, Phys. Fluids 19 (2007) 047101.
[8] M.O. Lamminen, H.W. Walker, L.K. Weavers, Mechanisms and factors influencing the ultrasonic cleaning of particle-fouled ceramic membranes, J. Membrane Sci. 237 (2004) 213–223.
[9] P. Prentice, A. Cuschierp, K. Dholakia, M. Prausnitz, P. Campbell, Membrane disruption by optically controlled microbubble cavitation, Nat. Phys. 1 (2005) 107–110.
[10] D. Chen, L.K. Weavers, H.W. Walker, Ultrasonic control of ceramic membrane fouling by particles: effect of ultrasonic factors, Ultrason. Sonochem. 13 (2006) 379–387.
[11] A. Zijlstra, T. Janssens, K. Wostyn, M. Versluis, P.M. Mertens, D. Lohse, High speed imaging of 1 MHz driven microbubbles in contact with a rigid wall, Solid State Phenom 145–146 (2009) 7–10.
[12] Y. Hagimoto, K. Asada, H. Iwamoto, in: Proceedings of 2005 IEEE International Symposium on Semiconductor Manufacturing, San Jose, CA, 2005, p. 215.
[13] T.G. Leighton, The Acoustic Bubble, Academic, London, 1994.
[14] H. Kuttruff, Ultrasonics Fundamentals and Applications, Elsevier, London, 1991.
[15] H. Krupp, Particle adhesion: theory and experiment, Adv. Colloid Interf. Sci. 1 (1967) 111–239.
[16] F. Zhang, A.A. Busnaina, M.A. Fury, S. Wang, The removal of deformed submicron particles from silicon wafers by spin rinse and megasonics, J. Electron. Mater. 29 (2000) 199–204.
[17] J. Israelachvili, Intermolecular and Surface Force, Academic Press, London, 1992.
[18] C. Tsai, D.Y.H. Pui, B.Y.H. Liu, Capture and rebound of small particles upon impact with solid surfaces, Aerosol Sci. Technol. 12 (1990) 497–507.
[19] V.A. Parsegian, G.H. Weiss, Spectroscopic parameters for computation of van der waals forces, J. Colloid Interf. Sci. 81 (1981) 285–289.
[20] J. Visser, On Hamaker constants: a comparison between Hamaker constants and Lifshitz–van der Waals constants, Adv. Colloid Interf. Sci. 3 (1972) 331–363.
[21] S.P. Timoshenko, J.N. Goodier, Theory of Elasticity, McGraw-Hill, New York, 1970.
[22] U. Holzwarth, H. Stamm, Mechanical and thermomechanical properties of commercially pure chromium and chromium alloys, J. Nucl. Mater. 300 (2002) 161–177.